



## OPEN ACCESS

## EDITED BY

Mukesh Kumar Gupta,  
National Institute of Technology Rourkela, India

## REVIEWED BY

Paolo Zambonelli,  
University of Bologna, Italy  
Yongzhen Huang,  
Northwest A&F University, China

## \*CORRESPONDENCE

Wei Peng  
✉ pengwei0112@sohu.com

<sup>†</sup>These authors have contributed equally to this work

RECEIVED 03 August 2023

ACCEPTED 02 October 2023

PUBLISHED 17 October 2023

## CITATION

Luo M, Wang H, Zhang J, Yixi K, Shu S, Fu C, Zhong J and Peng W (2023) IMF deposition ceRNA network analysis and functional study of HIF1 $\alpha$  in yak.  
*Front. Vet. Sci.* 10:1272238.  
doi: 10.3389/fvets.2023.1272238

## COPYRIGHT

© 2023 Luo, Wang, Zhang, Yixi, Shu, Fu, Zhong and Peng. This is an open-access article distributed under the terms of the [Creative Commons Attribution License \(CC BY\)](#). The use, distribution or reproduction in other forums is permitted, provided the original author(s) and the copyright owner(s) are credited and that the original publication in this journal is cited, in accordance with accepted academic practice. No use, distribution or reproduction is permitted which does not comply with these terms.

# IMF deposition ceRNA network analysis and functional study of HIF1 $\alpha$ in yak

Mengning Luo<sup>1†</sup>, Hui Wang<sup>1†</sup>, Jun Zhang<sup>2</sup>, Kangzhu Yixi<sup>1</sup>, Shi Shu<sup>2</sup>, Changqi Fu<sup>2</sup>, Jincheng Zhong<sup>1</sup> and Wei Peng<sup>2\*</sup>

<sup>1</sup>Key Laboratory of Qinghai-Tibetan Plateau Animal Genetic Resource Reservation and Utilization, Sichuan Province and Ministry of Education, Southwest Minzu University, Chengdu, China, <sup>2</sup>Qinghai Academy of Animal Science and Veterinary Medicine, Qinghai University, Xining, China

The concentration of intramuscular fat (IMF) is a crucial determinant of yak meat quality. However, the molecular mechanisms that regulate IMF in yak remain largely elusive. In our study, we conducted transcriptome sequencing on the longissimus dorsi muscle tissues of yaks with varying IMF contents. We then filtered differentially expressed genes (DEGs), microRNAs (DEMs), and long non-coding RNAs (DELS) to elucidate potential regulatory pathways of adipogenesis in yaks. Overall, our research sheds light on an array of potential mRNAs and noncoding RNAs implicated in IMF deposition and elaborates on the role of HIF1 $\alpha$  in yaks. These findings contribute valuable insights that can serve as a guide for further research into the molecular mechanisms governing IMF deposition.

## KEYWORDS

IMF, adipogenesis, RNA-seq, HIF1 $\alpha$ , ceRNA, yak

## 1. Introduction

The yak (*Bos grunniens*), a distinctive bovine species native to the Qinghai-Tibet Plateau, is exceptionally adept at withstanding the severe local conditions, such as freezing temperatures and oxygen scarcity. Currently, China's yak population is estimated at 18 million, comprising roughly 18% of the country's beef cattle inventory. Yaks have served as a crucial livestock resource for herdsman, offering bountiful supplies of meat, milk, and fur, and playing a critical role in the socioeconomic structure of the local communities.

With the current trend toward health consciousness, high-quality, sustainable beef has garnered international attention (1, 2). Yet, the acceptability of yak meat is somewhat hampered by its low yield, dense muscle fibers, minimal intramuscular fat (IMF) content, and limited tenderness. The development of muscle and IMF are complex processes that contribute significantly to economic factors and meat quality. These developments begin early in bovine embryogenesis, with the proliferation of myoblast progenitors and mononuclear myoblasts forming multinuclear muscle fibers (3). Fat formation commences during the second trimester (4), stemming from the proliferation and differentiation of intramuscular preadipocytes. Thus, unraveling the genetic regulation mechanisms behind IMF formation and muscle development is of paramount importance to enhancing yak meat quality.

The content of IMF significantly influences beef's tenderness and juiciness, making its optimization a focal point of research (5). Various studies have identified numerous lipid metabolism-associated genes linked with IMF deposition, including adiponectin, C1Q and collagen domain containing (ADIPOQ) (6), peroxisome proliferator-activated receptor gamma (PPAR $\gamma$  or PPARG) (7), thyroid hormone responsive (8), and fatty acid-binding protein 4

(FABP4) (9). A genome-wide association study proposed that PPARG coactivator 1 alpha, hepatocyte nuclear factor 4 gamma, and forkhead box P3 are implicated in IMF deposition in cattle (9). Comparative transcriptome analysis identified Phosphoenolpyruvate Carboxykinase 1 (PCK1) as significantly associated with IMF (10). Our prior work identified several key genes involved in IMF deposition in yaks, including *LPL* (11), *ACADL* (11), *SCD* (11), *FASN* (11), *lncFAM200B* (12), and *miR-6529a* (12). Additionally, ChIP-seq and mRNA-seq showed that SIRT1 plays an epigenetic role in IMF deposition through H3K4ac in yaks (13). Despite numerous studies, the molecular mechanisms regulating IMF deposition in yaks remain elusive.

This study aims to identify and scrutinize functional genes related to IMF development in yak longissimus dorsi muscle. By combining analyses, we constructed a competitive endogenous RNA (ceRNA) regulatory network, through which we identified several potential miRNA-lncRNA-mRNA regulatory axes possibly related to IMF deposition. Finally, we confirmed the regulatory effect of a candidate gene, *HIF1α*, on the proliferation and differentiation of yak intramuscular preadipocytes.

## 2. Materials and methods

### 2.1. Ethics statement

This research was endorsed by the Committee for Animal Ethics of the College of Animal Science and Technology, Southwest Minzu University (Permit number: SMU 202106010). We ensured all experimental protocols complied with the guidelines set by the approving committee. We obtained written permission from the owner of the yak to take samples.

### 2.2. Sample collection

Samples were collected from Xiaojin County, located in Sichuan Province, China. Following the slaughter of yaks, longissimus dorsi tissues from 24 yaks were sterilely dissected and preserved in liquid nitrogen. The IMF content of each sample was ascertained following the standard Soxhlet extraction method. Subsequently, six samples - three highest IMF content ( $4.50 \pm 0.20$ ) (H-IMF) and three lowest IMF content ( $2.52 \pm 0.11$ ) (L-IMF) - were selected from 24 ( $3.50 \pm 0.68$ ) samples for total RNA extraction and sequencing.

### 2.3. Total RNA isolation, sequencing and data processing

The total RNA was extracted by TRIzol (Invitrogen, Virginia, USA) reagent according to the manufacturer's instructions. The extracted RNA was used for the lncRNA and miRNA library construction according to previous standard method. The RNA libraries (lncRNA and miRNA) were then sequenced by the Illumina HiSeqTM 4,000 (Gene Denovo, Guangzhou, China) platform. After completing the sequencing of the lncRNA library, we obtained data about both mRNA and lncRNA.

For lncRNA and mRNA sequencing results, quality control of raw reads was conducted using Fastp (V0.18.0) (14). We removed reads containing adaptors and unknown nucleotides (N) greater than 10%, as well as all low-quality reads with an overabundance of adenine bases (A) (> 50% base, Q value  $\leq 20$ ). This process resulted in high-quality clean reads, which served as the basis for all downstream analyses. Initially, Bowtie2 (V2.2.8) (15) was employed to align the clean reads to the yak ribosome database. Following the exclusion of the ribosomal reads, the remaining unmapped reads were used for subsequent transcriptome analysis. Next, we utilized HISAT2 (V2.1.0) (16) to conduct a comparative analysis based on the reference genome (Ensembl\_release100), and the transcripts were reconstructed with StringTie (V1.3.4). Finally, the differential expression patterns of lncRNAs and mRNAs were analyzed via the Gene Denovo platform. We normalized the expression levels of lncRNA and mRNA using the FPKM (fragments per kilobase of transcript per million mapped reads) method.

For miRNA analysis, we performed a series of filtering steps on the raw reads. These included removing reads containing 5' adaptors, low-quality reads (those with more than one base having a quality value of less than 20 or reads containing unidentified nucleotides), reads without insert fragments, reads with inserted fragments shorter than 18 nucleotides, and reads containing predominantly adenine bases (more than 70% of the bases in a read are A). These steps helped us secure high-quality reads. After removing duplicate reads, we aligned all unannotated tags with the reference genome and identified potential novel miRNA candidates. We calculated miRNA expression levels using transcripts per million (TPM) as a measure. The formula for TPM is as follows:  $TPM = T * 10^6 / N$ , where T represents the tags of miRNA and N denotes the total miRNA tags (the sum of existing, existing editing, known, and newly identified miRNA counts).

### 2.4. Analysis of differentially expressed lncRNAs, mRNAs and miRNAs

DESeq2 (17) software was utilized to analyze the significance of lncRNAs and mRNAs, while the edgeR (18) package was employed for miRNA screening. The selection criteria for differentially expressed lncRNA, mRNA and miRNA were set as an expression level change of more than 1.5-fold, with a *p* value  $\leq 0.05$  between the H-IMF and L-IMF groups.

### 2.5. Prediction of target genes and functional enrichment analysis

The prediction of differentially expressed miRNAs (DEMs) targets was performed using miRanda (v3.3a) and TargetScan (Version:7.0) software. The common genes predicted by both databases were established as the final target genes for each DEM. Target prediction for differentially expressed lncRNAs (DELs) utilized three strategies: antisense, cis-acting and trans-acting regulation prediction. For antisense regulation, RNAplex software identified targets by comparing complementary bases between the lncRNA and mRNA. For cis-acting prediction, gene locations within a 10 kb radius of the lncRNA on the yak genome were identified as cis-acting

regulatory targets. For trans-acting targets, co-expression of lncRNA and mRNA, regardless of mRNA location, was a key determinant. LncTar was used to calculate free energy between lncRNA and mRNA to predict lncRNA targets.

The potential biological functions and regulatory pathways of differentially expressed mRNAs (DEGs), DEM targets and DEL targets were analyzed using Gene Ontology (GO) and Kyoto Encyclopedia of Genes and Genomes (KEGG) enrichment analyses, conducted with the R package ClusterProfiler (3.8.1) (19). Statistical significance was assigned at a  $p$  value  $\leq 0.05$ .

## 2.6. Construction of the ceRNA network

We calculated the Spearman rank correlation coefficient between miRNA and candidate ceRNAs (lncRNAs and mRNAs). We selected target gene pairs with a correlation coefficient of  $\leq -0.7$ . Pearson correlation coefficients between ceRNA pairs were also calculated. Pairs with a correlation coefficient greater than 0.9 were considered as potential ceRNA pairs. Based on these results, we performed a hypergeometric cumulative distribution function test. ceRNA pairs with a  $p$  value of  $\leq 0.05$  were chosen as the final ceRNA pairs. Finally, using Cytoscape software, we constructed a ceRNA regulation map.

## 2.7. RT-qPCR validation

The relative expression levels of genes were determined using the TB Green Premix EX Taq™ II kit (TaKaRa, Osaka, Japan) through quantitative reverse-transcription polymerase chain reaction (RT-qPCR). Primer information is provided in [Supplementary Table S1](#). We chose the  $\beta$ -actin gene as the normalization control for mRNAs and lncRNAs, and the U6 gene as the normalization control for miRNAs, and relative expression levels were computed using the  $2^{-\Delta\Delta Ct}$  method.

## 2.8. Construction of adenovirus and siRNA synthesis

Recombinant adenoviruses were created following a previously established procedure. Briefly, the cDNA of *HIF1 $\alpha$*  from yak was amplified and cloned into the pAV[Exp]-GFP-CMV vector (named Ad-*HIF1 $\alpha$* ). An adenoviral plasmid containing GFP (named Ad-*GFP*) served as the control. The small interfering RNA (siRNA) for *HIF1 $\alpha$*  (sense GCCGCUCAUUUAUGAAUATT, antisense UAUUCAUA AAUUGAGCGGCTT, named si-*HIF1 $\alpha$* ) and a negative control (sense UUCUCCGAACGUGUCACGUTT, antisense ACGUGACACG UUCGGAGAATT, named NC) were synthesized by Sigma (USA).

## 2.9. Cell culture and transfection

Cells were cultured in DMEM/F12 medium (Hyclone, USA), supplemented with 10% fetal bovine serum (Hyclone) and 1% penicillin–streptomycin (Boster, Switzerland), and incubated at 37°C with 5% CO<sub>2</sub>. Upon reaching 80% confluence, cells were serum-starved for 4h before siRNA transfection, carried out using

Lipofectamine™3000 reagent (Invitrogen) as per the manufacturer's instructions. Adenovirus was injected according to the formula: volume ( $\mu$ L) = MOI (1000) \* number of cells / adenovirus titers (IFU/ml) \* 1000. After transfection for 6h, the medium was replaced with induction medium (complete medium containing oleic acid), supplemented with 200  $\mu$ M cobalt (II) chloride hexahydrate (Sigma). Cells were harvested 48h later for subsequent experiments.

## 2.10. Oil Red O staining and intracellular triglyceride determination

Adherent cells in a 12-well plate were first gently washed with PBS solution. Subsequently, 400  $\mu$ L of 4% paraformaldehyde (Biosharp, China) was added to fix the cells for 1h at 20°C. Afterward, the fixative was removed by washing with PBS solution, and the cells were stained with Oil Red O reagent (Sigma). This reagent was prepared by dissolving it in isopropanol solution and diluted with PBS at a 3:2 ratio. After staining the fixed cells for 30min at 20°C, they were washed five times with PBS solution. The cells were then observed and photographed. Oil Red O dye was extracted with isopropyl alcohol and OD values were determined. The intracellular triglyceride (TG) levels were determined using a triglyceride assay kit (Applygen Technologies Inc., China) as per the manufacturer's instructions. Briefly, the total proteins were first extracted and detected using RIPI reagent (Beyotime, Shanghai, China) and a Pierce BCA protein assay kit (Thermo Fisher Scientific, Massachusetts, USA), respectively. The intracellular TG was then detected and the content was normalized to the total protein content.

## 2.11. CCK-8 assay

The CCK-8 assay was employed to analyze cell proliferation. Cells were inoculated in a 96-well plate and cultured in fresh complete medium for 0, 24, 48, 72, and 96h, respectively. Ten microliters of CCK-8 reagent was added to each well and incubated for 2h at 37°C. Absorbance was measured at 480nm wavelength after returning to room temperature.

## 2.12. Statistical analysis

One-way ANOVA was performed using SPSS (version 25.0; IBM Corp, Armonk, NY, USA), and the significance was determined using Duncan's test. Significance was reported at  $p \leq 0.05$ . The data are presented as Mean  $\pm$  SD (standard deviation) from three biological replicates and three technical replicates. Indicators \*\*\* signify  $p < 0.001$ , \*\* denote  $p < 0.01$ , and \* represent  $p < 0.05$ .

# 3. Results

## 3.1. Overview of sequencing results

The lncRNA sequencing results yielded an average of 773,801,889 raw reads for the H-IMF group and 89,708,014 raw reads for the L-IMF group ([Figure 1A](#); [Supplementary Table S2](#)). Following quality

control, an average of 77,201,181 (99.77%) and 89,469,916 (99.73%) clean reads were obtained for the respective groups (Figure 1B; Supplementary Table S2). Approximately 91.29 to 92.85% of the clean reads were successfully mapped to the yak reference genome. Out of these, 73.33 to 76.47% of the reads were uniquely mapped to specific regions of the genome, while 15.83 to 17.99% showed multiple genomic locations (Supplementary Table S2). These findings demonstrate the reliability of the sequencing data obtained from the longissimus dorsi muscle of yak, making it suitable for subsequent bioinformatics analysis. The even distribution of a large number of reads across the genes indicates high sample quality. Furthermore, the ratio of reads corresponding to exons, introns, and intergenic regions varied, with exons exhibiting the highest ratio and intergenic regions showing the lowest (Figure 1C). These results suggest that the RNA expression profiles differ among the various samples, indicating specific gene regulation patterns.

For the miRNA sequencing results, we generated a total of 980,758 and 187,527,38 clean reads from the longissimus dorsi muscle of yak

in the H-IMF and L-IMF groups, respectively (Supplementary Table S3). Following the removal of low-quality reads and adapter sequences, we obtained 936,603,2 and 162,650,62 clean tags for further analysis (Supplementary Table S3). Of these, 156,302 and 255,847 clean tags were mapped to the yak reference genome, respectively. Tags mapped to exons, introns, and repetitive sequences were excluded (Figure 1F; Supplementary Table S3). Most of the small RNA ranged from 18 to 25 nt, with 22 nt being the most common length (Figure 1D). We identified a total of 1,073 miRNAs for subsequent analysis (Figure 1E).

### 3.2. Differential expression analysis of mRNAs

We screened the DEGs between the H-IMF and L-IMF groups, yielding 469 DEGs, with 318 upregulated and 151 downregulated (Figure 2A; Supplementary Table S4). These included lipid

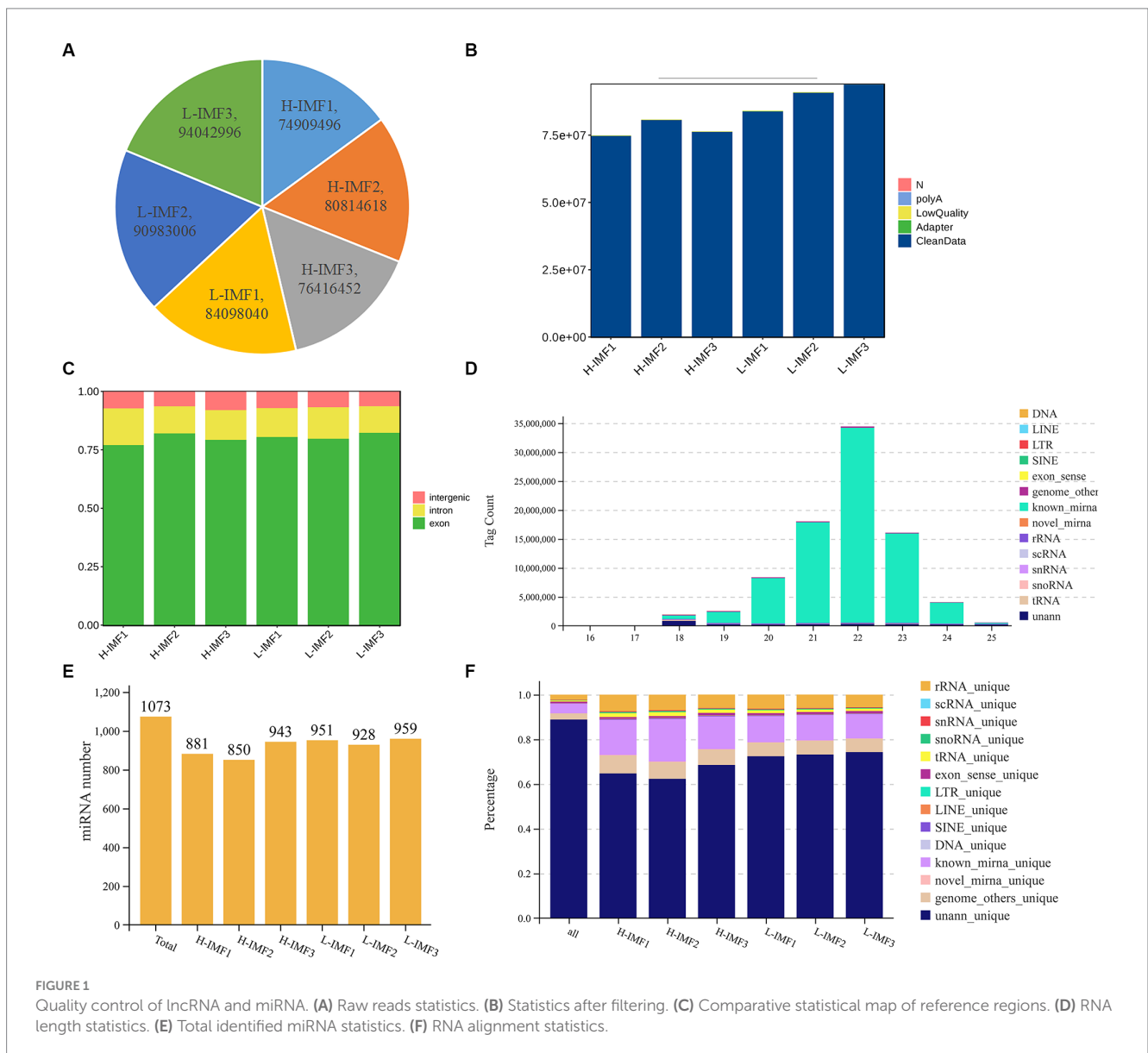


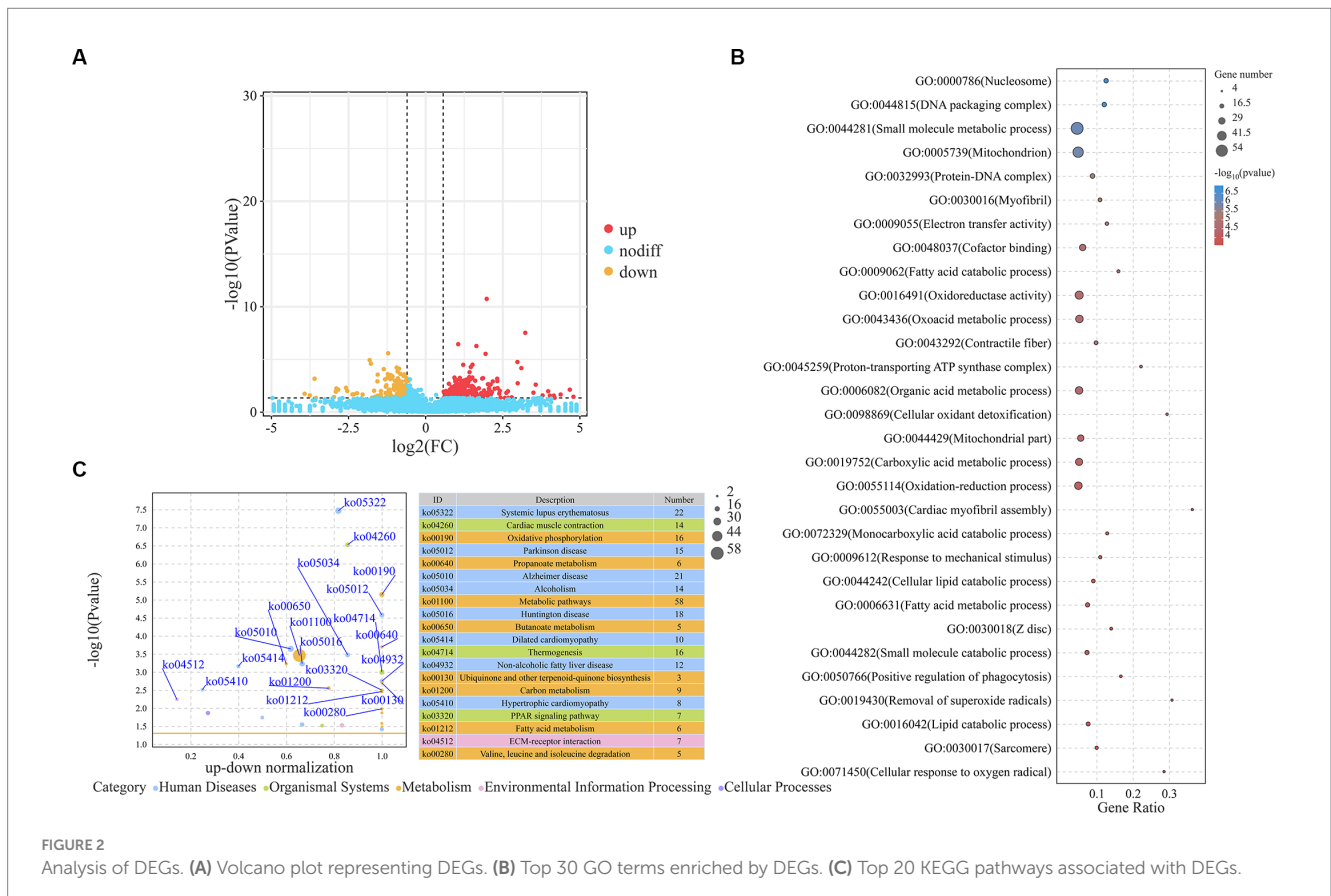
**FIGURE 1** Quality control of lncRNA and miRNA. (A) Raw reads statistics. (B) Statistics after filtering. (C) Comparative statistical map of reference regions. (D) RNA length statistics. (E) Total identified miRNA statistics. (F) RNA alignment statistics.

metabolism-related genes such as galactosidase beta 1 like 2 (*GLB1L2*,  $\log_2FC = -2.36$ ), APC regulator of WNT signaling pathway 2 (*APC2*,  $\log_2FC = -1.21$ ), heart Fatty acid-binding protein (*H-FABP*,  $\log_2FC = 2$ ), phospholipid phosphatase related 2 (*PLPPR2*,  $\log_2FC = 1.88$ ), and ELOVL fatty acid elongase 6 (*ELOVL6*,  $\log_2FC = 1.64$ ). Muscle development-related genes were also included, such as methyltransferase like 21C (*METTL21C*,  $\log_2FC = -2.56$ ), myosin light chain 3 (*MYL3*,  $\log_2FC = 3.12$ ), and myosin IG (*MYO1G*,  $\log_2FC = 1.06$ ) (Figure 2B; Supplementary Table S5). GO analysis revealed that these DEGs were enriched in lipid metabolism terms, such as regulation of the MAPK cascade (GO:0043408), fatty acid metabolic process (GO:0006631), lipid catabolic process (GO:0016042), fatty acid catabolic process (GO:0009062), lipid oxidation (GO:0034440), fatty acid derivative metabolic process (GO:1901568), and Wnt-protein binding (GO:0017147), as well as muscle development terms, including muscle fiber development (GO:0048747), striated muscle cell development (GO:0055002), muscle tissue development (GO:0060537), and muscle cell development (GO:0055001) (Supplementary Table S6). KEGG analysis revealed that DEGs were significantly annotated in lipid metabolism-related pathways such as metabolic pathways (ko01100), fatty acid metabolism (ko01212), PPAR signaling pathway (ko03320), valine, leucine and isoleucine degradation (ko00280), and fatty acid degradation (ko00071). They were also annotated in muscle development-related pathways, such as cardiac muscle contraction (ko04260) (Figure 2C; Supplementary Table S7).

### 3.3. Differential expression analysis of miRNAs

We identified a total of 57 DEMs between the H-IMF and L-IMF groups, with 20 upregulated and 37 downregulated (Figure 3A; Supplementary Table S8). We then predicted the targets of these DEMs (Supplementary Table S9) and performed GO and KEGG analyses. GO analysis indicated that the targets of the DEMs were significantly enriched in lipid metabolism-related terms, including ATP binding (GO:0005524), fatty acid biosynthetic process (GO:0006633), phosphatidylinositol binding (GO:0035091), saturated fatty acid elongation (GO:0019367), and very long-chain fatty acid biosynthetic process (GO:0042761) (Figure 3B; Supplementary Table S10).

KEGG pathway analysis showed that the targets of the DEMs were enriched in several signaling and metabolic pathways. These included the MAPK signaling pathway (ko04010), PI3K-Akt signaling pathway (ko04151), FoxO signaling pathway (ko04068), adipocytokine signaling pathway (ko04920), fatty acid metabolism (ko01212), and HIF-1 signaling pathway (ko04066) (Supplementary Table S11). Additionally, we noted enrichment in pathways related to muscle development, such as the regulation of actin cytoskeleton (ko04810), arrhythmogenic right ventricular cardiomyopathy (ko05412), hypertrophic cardiomyopathy (ko05410), and vascular smooth muscle contraction (ko04270) (Figure 3C; Supplementary Table S11).



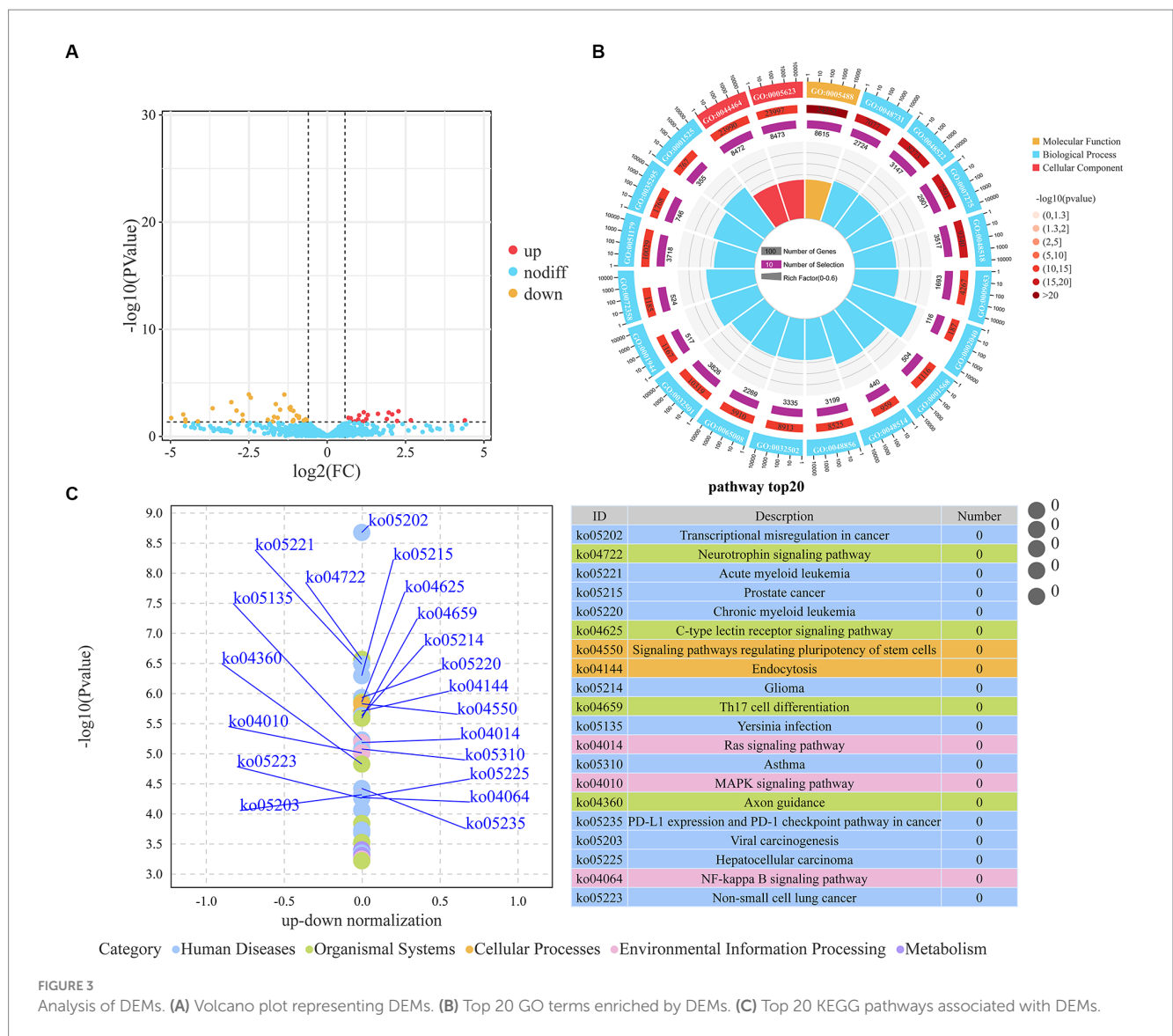


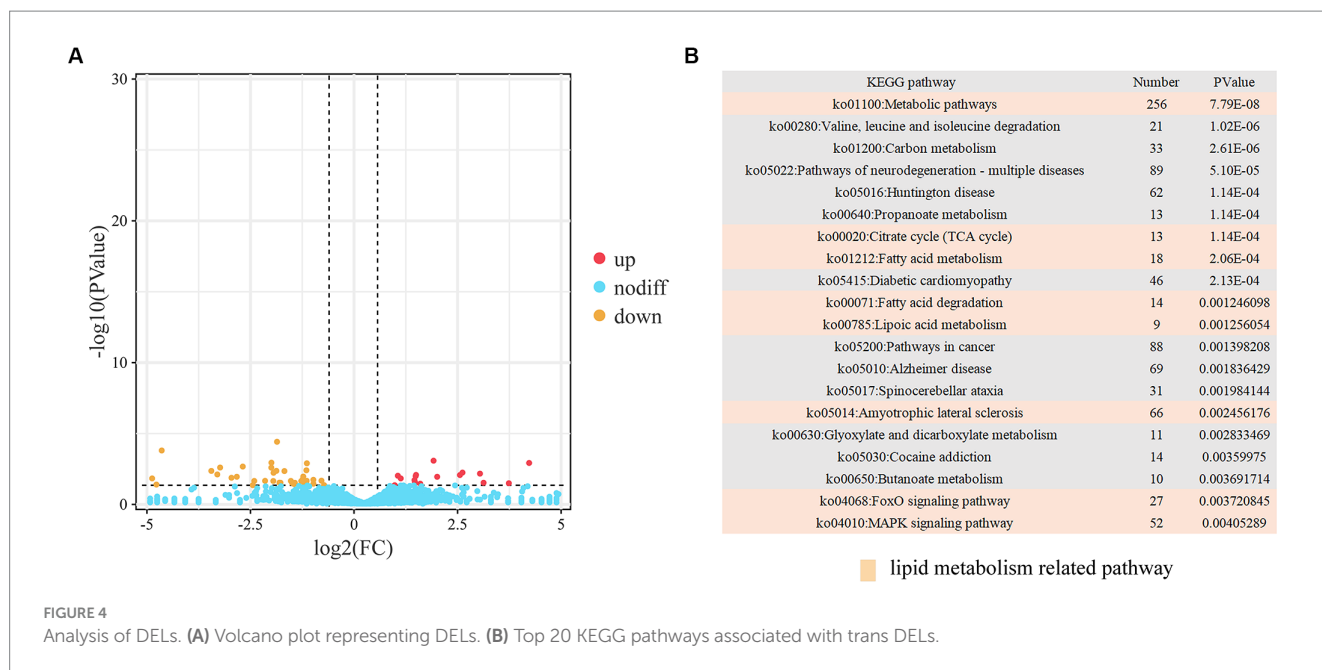
FIGURE 3 Analysis of DEMs. (A) Volcano plot representing DEMs. (B) Top 20 GO terms enriched by DEMs. (C) Top 20 KEGG pathways associated with DEMs.

### 3.4. Differential expression analysis of lncRNAs

We identified a total of 73 DELs, including 25 upregulated and 48 downregulated (Figure 4A; Supplementary Table S12). The targets of these lncRNAs were predicted using three independent algorithms, antisense, cis, and trans. From this analysis, 3,762 target genes were identified. Specifically, 10 genes were found to be targets of 11 antisense lncRNAs, 47 genes were targeted by 45 cis-acting lncRNAs, and 3,705 genes were targeted by 73 trans-acting lncRNAs. Subsequently, we performed KEGG pathway analysis on the identified target genes. The results revealed a significant enrichment in pathways related to both lipid metabolism (such as butanoate metabolism, fatty acid metabolism, PPAR signaling pathway, insulin secretion, and fatty acid degradation) and muscle development (including cardiac muscle contraction, adrenergic signaling in cardiomyocytes, hypertrophic cardiomyopathy, dilated cardiomyopathy, and regulation of actin cytoskeleton) (Figure 4B; Supplementary Table S13).

### 3.5. Construction of the ceRNA network and RT-qPCR validation of gene expression

There is mounting evidence indicating that both mRNA and lncRNA can function as ceRNAs for specific miRNAs, playing key roles in regulating gene function across various processes (20). This suggests potential co-regulation of ceRNAs and their corresponding miRNAs in IMF deposition. Integrating the identified lncRNA-mRNA pairs, we constructed a comprehensive ceRNA network. This network encompasses 16 DEGs, 11 DEMs, and 12 DELs, reflecting 26 interaction relationships (Figure 5A). The 16 identified genes were primarily enriched in metabolic pathways (ko01100), valine, leucine, and isoleucine degradation (ko00280), cardiac muscle contraction (ko04260), motor proteins (ko04814), and hypertrophic cardiomyopathy (ko05410) (Supplementary Table S14). Within this network, both MSTRG.12131.3 and its target *ENSBGRG0000010263* were found to be targeted by novel-m0258-5p and novel-m0259-5p. Additionally, *CREG1* and *ECHDC3* are regulated by miR-3059-x. Similar regulatory dynamics were observed in the



miR-10162-x-ENSBGRT00000028385-ENSBGRG00000000535 and miR-1285-z-MSTRG.347.2-ENSBGRG00000013053 ceRNA sub-networks, implying that *ENSBGRG00000010263*, *ENSBGRG0000000535*, *ENSBGRG00000013053*, *CREG1*, and *ECHDC3* could be crucial genes modulated by noncoding RNAs in regulating IMF deposition.

To validate the RNA-Seq results, we performed RT-qPCR on a random selection of RNAs. These included five mRNAs (*SMIM8*, *FBXO17*, *MYL3*, *ECHDC3*, and *ENSBGRG0000000535*) (Figure 5B), four lncRNAs (MSTRG.13598.1, MSTRG.8133.1, MSTRG.8121.1, and *ENSBGRT00000028385*) (Figure 5C), and one miRNA (miR-3059-x) (Figure 5D). The expression levels of these selected RNAs significantly varied in the longissimus dorsi muscle of yaks with differing fat content. Furthermore, the observed expression patterns were highly congruent with the results acquired via the RNA-Seq approach.

### 3.6. Investigation of *HIF1α*'s effect on yak intramuscular preadipocyte proliferation and differentiation

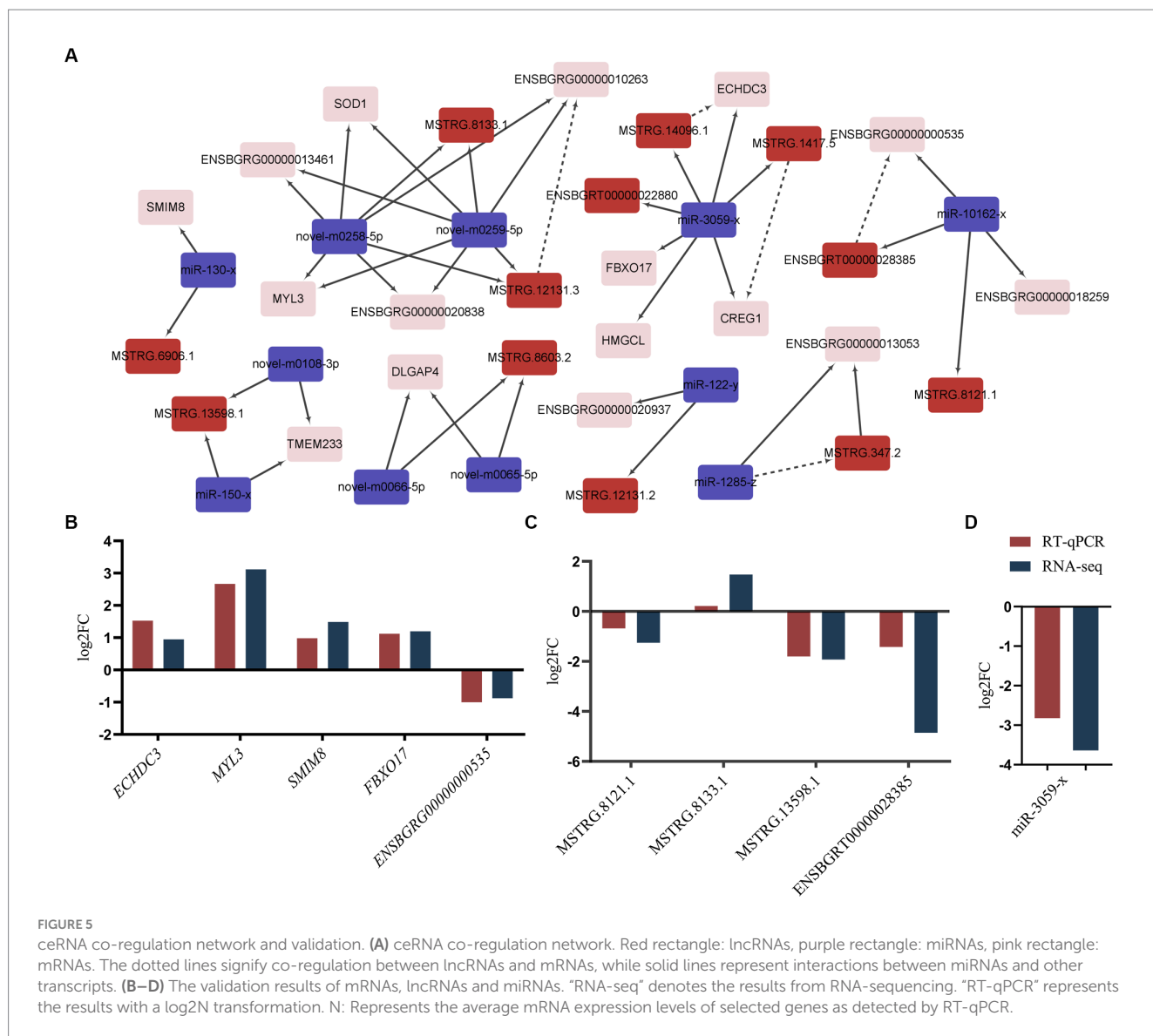
Our sequencing results indicated that 109 target genes of DEMs were significantly enriched in the HIF-1 signaling pathway (ko04066), such as *HIF1α*, *IGF1*, *ARNT*, *PIK3CA*, *AKT3*, *STAT3* and *MAPK1* (Supplementary Table S11). It has been reported that the hypoxia-inducible factor (*HIF1α*) acts as a key factor in lipid metabolism (21). Consequently, we decided to investigate the effects of *HIF1α* on the proliferation and differentiation of yak intramuscular preadipocytes, employing adenovirus-mediated overexpression and siRNA-mediated interference techniques. Our RT-qPCR results (Figures 6A,B) indicated that the inhibition of *HIF1α* significantly reduced its mRNA level ( $p < 0.001$ ). Conversely, the expression levels of proliferation-related genes *ki67* ( $p < 0.001$ ) and *PCNA* ( $p < 0.05$ ) were increased. However, an opposite trend was observed following the overexpression treatment (Figures 6A,B). We also utilized 200 μM Cobalt(II) chloride hexahydrate (22) to simulate a hypoxic environment and subsequently

assessed cell proliferation. The results revealed that cell proliferation activity significantly increased after *HIF1α* inhibition and decreased following its overexpression (Figures 6C,D). These findings suggest that *HIF1α* may positively influence the proliferation of intramuscular preadipocytes in yaks.

To evaluate the influence of *HIF1α* on the differentiation of intramuscular preadipocytes, we assessed the expression of differentiation-associated genes, namely *PPARγ* (23), *C/EBPα* (24), and *FABP4* (25), following either inhibition or overexpression of *HIF1α*. Our results revealed that the mRNA levels of *C/EBPα* were significantly downregulated ( $p < 0.01$ ), while *FABP4* was notably enhanced ( $p < 0.05$ ) following *HIF1α* knockdown compared to control cells (Figure 7A). Conversely, *HIF1α* overexpression significantly upregulated the expression of *C/EBPα* ( $p < 0.01$ ) (Figure 7B). Under hypoxic conditions, lipid droplet formation was substantially reduced when *HIF1α* was inhibited (Figures 7C,D,F). In contrast, lipid droplet formation was significantly increased when *HIF1α* expression was enhanced (Figures 7C,E,G). These findings suggest that *HIF1α* might promote the differentiation of intramuscular preadipocytes in yaks.

## 4. Discussion

IMF, the fat accumulated between muscle fibers and within muscle cells, consists primarily of phospholipids and triglycerides. It is a crucial determinant of meat quality. Understanding the molecular mechanisms governing IMF deposition carries significant implications for animal husbandry. In this study, we initially identified 469 DEGs, 57 DEMs, and 73 DELs by sequencing the longissimus dorsi muscle of yaks with different IMF content. Subsequently, we predicted the targets of these DEMs and DELs. Remarkably, a substantial number of these DEGs, DEMs, and DELs were found to be enriched in pathways related to lipid metabolism and muscle development following functional annotation. Furthermore, many of these DEGs had known functions in lipid metabolism, such as *GLB1L2*, *APC2*, *H-FABP*, *PLPPR2*, and *ELOVL6*, and muscle development, including *METTL21C*, *MYL3*, and



*MYO1G*. These genes likely represent some of the determinants of yak fat content, and their genetic functions within yaks are worth further investigation. The ceRNA hypothesis has garnered considerable attention in recent years. An increasing number of studies are endeavoring to construct ceRNA networks associated with non-coding RNAs during adipogenesis (26–28). In this study, we assembled a ceRNA network in yaks’ longissimus dorsi muscle, exhibiting varied IMF levels, and analyzed the potential adipogenic regulatory effects of these lncRNAs, miRNAs, and mRNAs. Overall, we constructed a ceRNA regulatory network encompassing 12 miRNAs, 11 lncRNAs, and 16 mRNAs. Within this network, it was apparent that four genes associated with lipid metabolism (*CREG1*, *ECHDC3*, *HMGCL*, and *FBXO17*) were targeted by miR-3059-x. Recent studies have reported that *CREG* heterozygous mice, when fed a high-fat diet, exhibited significant obesity and a 30% increase in body weight compared to their wild-type counterparts (29). Further, liver-specific knockout of *CREG*, coupled with a high-fat diet, led to liver steatosis, obesity, and insulin resistance (30). The Enoyl-CoA hydratase (ECH) is a pivotal mitochondrial enzyme involved in fatty acid β-oxidation, catalyzing the

addition of H<sub>2</sub>O across the double bond of trans-2-enoyl-CoA, which forms a β-hydroxyacyl-CoA (31). Enoyl-CoA Hydratase Domain-Containing 3 (*ECHDC3*), a member of the ECH family, plays a regulatory role in adipocyte fatty acid metabolism, with *ECHDC3* silencing in human adipocytes significantly reducing insulin-stimulated glucose uptake and Akt Ser473 phosphorylation (32). The 3-hydroxy-3-methylglutaryl (HMG) CoA lyase (*HMGCL*) is a key enzyme in ketone body formation and is closely associated with energy metabolism (33). Meanwhile, the F-box protein (*FBXO17*) may inhibit the Wnt/β-catenin signaling pathway, thus influencing cancer progression (34). Our data demonstrated that these genes were differentially expressed in the longissimus dorsi muscle of yaks with differing fat content. Therefore, we hypothesize that the four identified genes (*CREG1*, *ECHDC3*, *HMGCL*, and *FBXO17*) and three new genes (*ENSBGRG00000010263*, *ENSBGRG00000000535*, and *ENSBGRG00000013053*) may play integral roles in regulating IMF deposition.

Furthermore, we identified several potential regulatory miRNAs (miR-1285-z, miR-122-y, miR-150-x, and miR-130-x). The principal

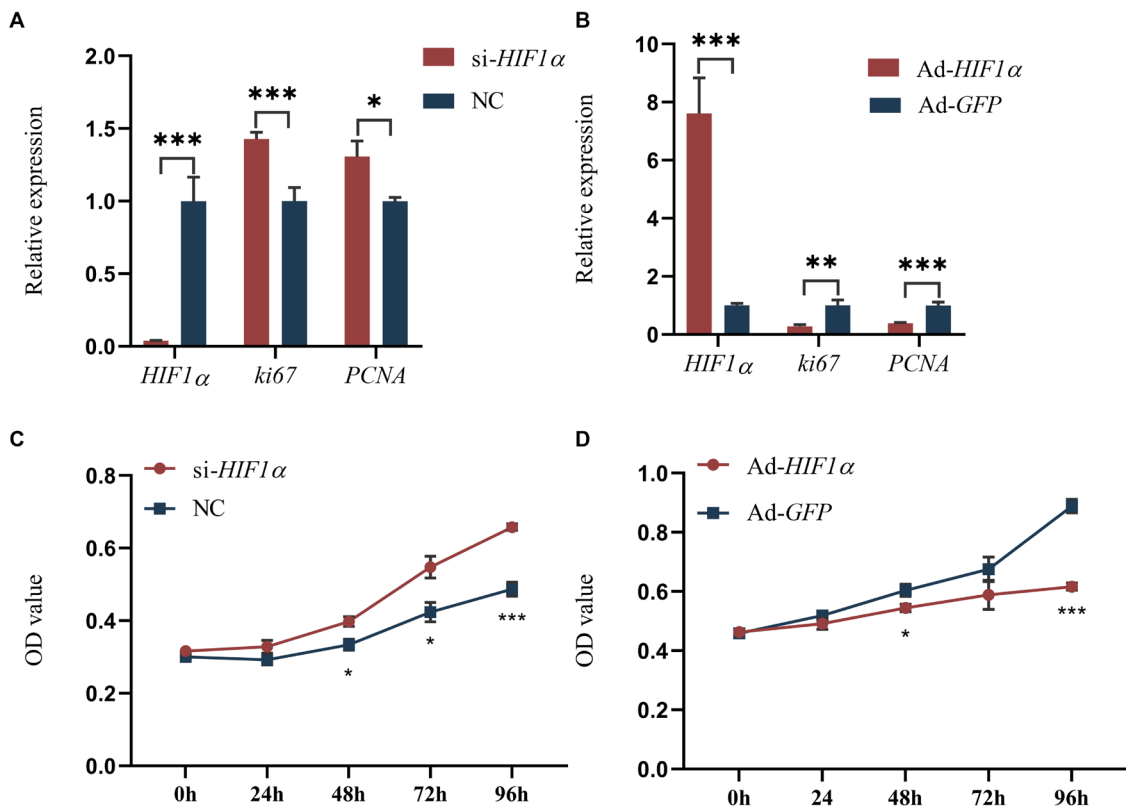


**FIGURE 6** Impact of *HIF1α* on yak intramuscular preadipocyte proliferation. (A,B) Results from RT-qPCR. (C,D) CCK-8 outcomes post-transfection with si-*HIF1α* or Ad-*HIF1α* at intervals of 0, 24, 48, 72, and 96 h. Indicators \*\*\* signify  $p < 0.001$ , \*\* denote  $p < 0.01$ , and \* represent  $p < 0.05$ .

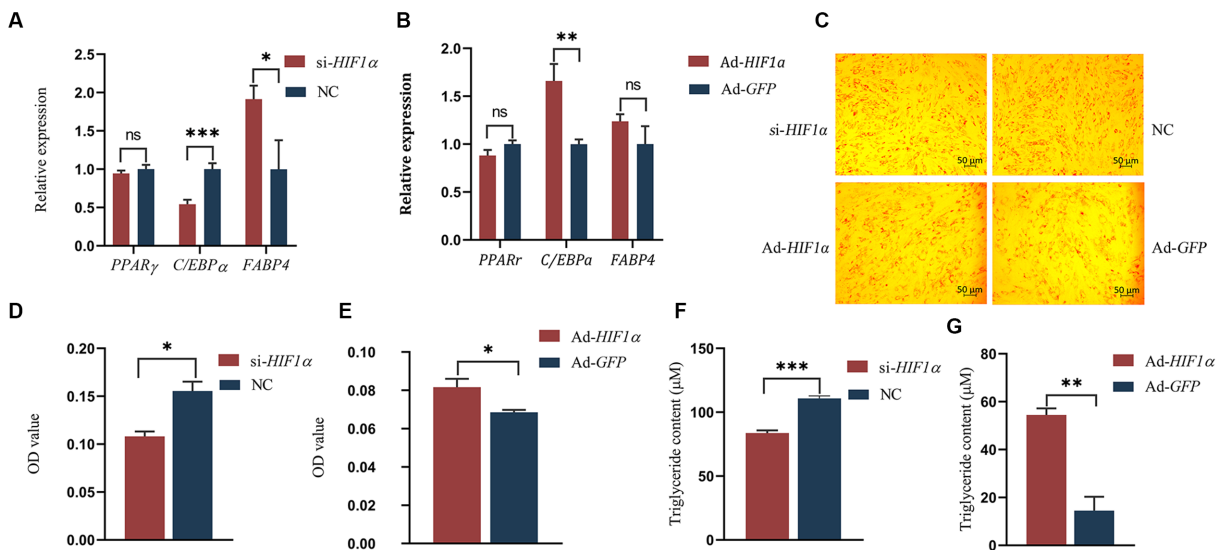


**FIGURE 7** Impact of *HIF1α* on differentiation of yak intramuscular preadipocytes. (A,B) RT-qPCR results. (C–E) Oil Red O staining results post-transfection with si-*HIF1α* or Ad-*HIF1α* for 48 h. (F,G) TG test results. Indicators \*\*\* signify  $p < 0.001$ , \*\* denote  $p < 0.01$ , and \* represent  $p < 0.05$ .

biological function of miRNAs is carried out through pairing with a complementary site in the 3'UTR of their target mRNA, leading to post-transcriptional regulation by inhibiting translation. Most current

research on miR-1285 concentrates on cancers, such as lung squamous cell carcinoma (35) and thyroid tumors (36). It has been found that TPI1, a pivotal enzyme in the glycolysis pathway, is a functional target

of miR-1285-3p, and miR-1285-3p can diminish *TPI1* expression in Sertoli cells (37). Another study established that inhibiting miR-122 safeguards hepatocytes from lipid metabolic disorders such as NAFLD and curbs lipogenesis by elevating Sirt1 and activating the AMPK pathway (38). Moreover, mice with a knockout of miR-150 exhibited metabolic advantages including reduced body weight, decreased energy intake, and augmented lipid metabolism (39). In a study related to bovine adipogenesis, it was reported that bta-miR-130a/b could influence bovine adipocyte differentiation by targeting *PPARG* and Cytochrome P4502U1 (*CYP2U1*) (40). Interestingly, the miRNAs mentioned above showed significant differential expression between high-IMF and low-IMF samples in our study, suggesting that miR-1285-z, miR-122-y, miR-150-x, miR-130-x, and miR-3059-x may be implicated in the IMF deposition of yaks. In the ceRNA sub-networks we constructed, MSTRG.12131.3 and its target *ENSBGRG0000010263* communicated via the shared novel-m0258-5p and novel-m0259-5p response elements, whereas MSTRG.14096.1 and its target *ECHDC3*, and MSTRG.1417.5 and its target *CREG1* both communicated via miR-3059-x response elements. However, *ENSBGRT0000028385* and its target *ENSBGRG0000000535*, and MSTRG.347.2 and its target *ENSBGRG0000013053* communicated via miR-10162-x and miR-1285-z response elements, respectively. Consequently, we hypothesize that these six sub-networks may play critical roles in the regulation of yak IMF deposition.

HIF1 $\alpha$ , a transcription factor, is composed of a regulatory 120 kDa  $\alpha$  subunit and a 91–94 kDa  $\beta$  subunit, also known as ARNT (41). Under normoxic conditions, oxygen induces the hydroxylation of conserved proline residues (Pro402 and Pro564) in HIF1 $\alpha$  subunits by oxygen-dependent HIF prolyl-4-hydroxylase domain enzymes (PHDs). This leads to the interaction with Von-Hippel-Lindau (VHL) protein, an ubiquitin ligase, and subsequent proteasomal degradation. Thus, HIF1 $\alpha$  has a relatively short half-life of about 5–10 min under normal oxygen conditions (42, 43). However, under hypoxic conditions, cells lack sufficient O<sub>2</sub>, inhibiting HIF1 $\alpha$  hydroxylation. This causes the HIF1 $\alpha$  subunit to stabilize and accumulate in the cytoplasm. Subsequently, the accumulated HIF1 $\alpha$  translocates to the nucleus, forming heterodimeric complexes with HIF-1 $\beta$ /ARNT (44, 45). This results in the recruitment and binding of p300/CBP to the hypoxia response element (HRE) in the promoter/enhancer region of the target gene, promoting its transcription. This process facilitates cellular response to hypoxia, crucial for maintaining oxygen homeostasis in the body (46–48). In recent years, the hypoxia adaptation mechanism of yaks, in which *HIF1 $\alpha$*  plays a significant role, has garnered increased attention (49, 50). Moreover, several studies have indicated that *HIF1 $\alpha$*  is implicated in hypoxia-induced lipid accumulation in hepatocytes (51), and is triggered by increased O<sub>2</sub> consumption in adipocytes (52). Intriguingly, the expression level of *HIF1 $\alpha$*  in yaks is significantly higher than that in cattle (53). *HIF1 $\alpha$*  serves as a crucial gene in lipid metabolism and is also a vital player in the adaptation to hypoxic conditions. Given the yak's remarkable ability to thrive in high-altitude, low-oxygen environments, we find the relationship between hypoxia-inducible factors like *HIF1 $\alpha$*  and low-fat characteristics to be a compelling subject for additional investigation. While *HIF1 $\alpha$*  is not part of our current ceRNA network study, it remains a focal point of our research agenda, warranting in-depth functional analysis. Moreover, our sequencing results revealed that 109 DEM targets were enriched in the HIF-1 signaling

pathway (ko04066). Consequently, we investigated the regulatory effect of *HIF1 $\alpha$*  on yak intramuscular preadipocytes. Cobalt chloride, a common model of chemical hypoxia (54), was employed. With the increase or inhibition of *HIF1 $\alpha$*  expression, mRNA levels of *FABP4* and *C/EBP $\alpha$* , excluding *PPAR $\gamma$* , were notably upregulated or downregulated. Combining the results of triglyceride measurements, oil red O stain, and CCK-8 assays, we concluded that *HIF1 $\alpha$*  negatively regulated the proliferation of yak intramuscular preadipocytes and positively influenced lipid droplet formation. These findings align with previous *HIF1 $\alpha$*  studies in other species (55–57). Notably, *CREG* may activate *HIF1 $\alpha$*  signaling via the inhibition of *VHL* expression (58). While its regulatory role in yak IMF deposition remains unclear, it provides a fresh perspective for future research.

## 5. Conclusion

Our study utilized high-throughput sequencing to analyze a large scale of differentially expressed mRNAs, miRNAs, and lncRNAs in longissimus dorsi muscle of yaks with high and low IMF content. Further, we constructed a ceRNA regulatory network based on the differentially expressed transcripts. Our findings revealed the genetic regulatory mechanisms and provided valuable data for understanding the low-fat traits of yaks. Additionally, we identified the regulatory role of *HIF1 $\alpha$*  in lipid deposition and the proliferation of yak intramuscular preadipocytes. This discovery is particularly important for studying both the low-fat characteristics and the hypoxic adaptation of yaks.

## Data availability statement

The datasets presented in this study can be found in online repositories. The names of the repository/repositories and accession number(s) can be found in the article/[Supplementary material](#).

## Ethics statement

The part of the study involving animal samples was reviewed and approved by the Institution Animal Care and Use Committee in the Southwest Minzu University (Permit number: SMU 202106010 revised in 1 June 2021), Chengdu, China. The animal study was approved by the Institution Animal Care and Use Committee in the Southwest Minzu University. The study was conducted in accordance with the local legislation and institutional requirements.

## Author contributions

ML: Data curation, Formal analysis, Investigation, Methodology, Validation, Visualization, Writing – original draft, Writing – review & editing. HW: Conceptualization, Funding acquisition, Methodology, Resources. JZ: Funding acquisition, Resources, Writing – review & editing. KY: Funding acquisition, Resources, Writing – review & editing. SS: Funding acquisition, Resources, Writing – review & editing. CF: Funding acquisition, Resources, Writing – review & editing. JZ: Funding acquisition, Resources, Writing – review & editing. WP: Funding acquisition, Resources, Writing – review & editing.

## Funding

The author(s) declare financial support was received for the research, authorship, and/or publication of this article. This work was supported by the National Natural Science Foundation of China (no. 31902153), the Qinghai Science and Technology Program, China (no. 2022-NK-110), the Program of National Beef Cattle and Yak Industrial Technology System (no. CARS-37), and the Fundamental Research Funds for the Central Universities, Southwest Minzu University (2022NYXXS049). The funders had no role in study design, data collection and analysis, decision to publish, or preparation of the manuscript.

## Acknowledgments

The authors thank the Key Laboratory of Qinghai-Tibetan Plateau Animal Genetic Resource Reservation and Utilization (Sichuan Province and Ministry of Education) of Southwest Minzu University for providing the experimental platform and conditions.

## References

1. Gerbens F, Verburg FJ, Van Moerkerk HT, Engel B, Buist W, Veerkamp JH, et al. Associations of heart and adipocyte fatty acid-binding protein gene expression with intramuscular fat content in pigs. *J Anim Sci.* (2001) 79:347–54. doi: 10.2527/2001.792347x
2. Fernandez X, Monin G, Talmant A, Mourot J, Lebre B. Influence of intramuscular fat content on the quality of pig meat-1. Composition of the lipid fraction and sensory characteristics of m. longissimus lumborum. *Meat Sci.* (1999) 53:59–65. doi: 10.1016/S0309-1740(99)00037-6
3. Shen X, Tang J, Ru W, Zhang X, Huang Y, Lei C, et al. CircINSR regulates fetal bovine muscle and fat development. *Front Cell Dev Biol.* (2021) 8:615638. doi: 10.3389/fcell.2020.615638
4. Sanchez-Gurmaches J, Guertin DA. Adipocyte lineages: tracing back the origins of fat. *Biochim Biophys Acta.* (2014) 1842:340–51. doi: 10.1016/j.bbdis.2013.05.027
5. Hausman GJ, Dodson MV, Ajuwon K, Azain M, Barnes KM, Guan LL, et al. The biology and regulation of preadipocytes and adipocytes in meat animals. *J Anim Sci.* (2009) 87:1218–46. doi: 10.2527/jas.2008-1427
6. Wang YH, Bower NI, Reverter A, Tan SH, De Jager N, Wang R, et al. Gene expression patterns during intramuscular fat development in cattle. *J Anim Sci.* (2009) 87:119–30. doi: 10.2527/jas.2008-1082
7. De Jager N, Hudson NJ, Reverter A, Barnard R, Café LM, Greenwood PL, et al. Gene expression phenotypes for lipid metabolism and intramuscular fat in skeletal muscle of cattle. *J Anim Sci.* (2013) 91:1112–28. doi: 10.2527/jas.2012-5409
8. Hudson NJ, Reverter A, Greenwood PL, Guo B, Café LM, Dalrymple BP. Longitudinal muscle gene expression patterns associated with differential intramuscular fat in cattle. *Animal.* (2015) 9:650–9. doi: 10.1017/S1751731114002754
9. Ramayo-Caldas Y, Fortes MR, Hudson NJ, Porto-Neto LR, Bolormaa S, Barendse W, et al. A marker-derived gene network reveals the regulatory role of PPARGC1A, HNF4G and FOXP3 in intramuscular fat deposition of beef cattle. *J Anim Sci.* (2014) 92:2832–45. doi: 10.2527/jas.2013-7484
10. Huang J, Feng X, Zhu R, Guo D, Wei Y, Cao X, et al. Comparative transcriptome analysis reveals that PCK1 is a potential gene affecting IMF deposition in buffalo. *BMC Genomics.* (2020) 21:710. doi: 10.1186/s12864-020-07120-w
11. Wang H, Zhong J, Zhang C, Chai Z, Cao H, Wang J, et al. The whole-transcriptome landscape of muscle and adipose tissues reveals the ceRNA regulation network related to intramuscular fat deposition in yak. *BMC Genomics.* (2020) 21:347. doi: 10.1186/s12864-020-6757-z
12. Ran H, Yang Y, Luo M, Liu X, Yue B, Chai Z, et al. Molecular regulation of yak preadipocyte differentiation and proliferation by *LncFAM200B* and ceRNA regulatory network analysis. *Cells.* (2022) 11:2366. doi: 10.3390/cells11152366
13. Ran H, He Q, Han Y, Wang J, Wang H, Yue B, et al. Functional study and epigenetic targets analyses of *SIRT1* in intramuscular preadipocytes via ChIP-seq and mRNA-seq. *Epigenetics.* (2023) 18:2135194. doi: 10.1080/15592294.2022.2135194
14. Chen S, Zhou Y, Chen Y, Gu J. Fastp: an ultra-fast all-in-one FASTQ preprocessor. *Bioinformatics.* (2018) 34:i884–90. doi: 10.1093/bioinformatics/bty560

## Conflict of interest

The authors declare that the research was conducted in the absence of any commercial or financial relationships that could be construed as a potential conflict of interest.

## Publisher's note

All claims expressed in this article are solely those of the authors and do not necessarily represent those of their affiliated organizations, or those of the publisher, the editors and the reviewers. Any product that may be evaluated in this article, or claim that may be made by its manufacturer, is not guaranteed or endorsed by the publisher.

## Supplementary material

The Supplementary material for this article can be found online at: <https://www.frontiersin.org/articles/10.3389/fvets.2023.1272238/full#supplementary-material>

15. Langmead B, Salzberg SL. Fast gapped-read alignment with bowtie 2. *Nat Methods.* (2012) 9:357–9. doi: 10.1038/nmeth.1923
16. Kim D, Langmead B, Salzberg SL. HISAT: a fast spliced aligner with low memory requirements. *Nat Methods.* (2015) 12:357–60. doi: 10.1038/nmeth.3317
17. Love MI, Huber W, Anders S. Moderated estimation of fold change and dispersion for RNA-seq data with DESeq2. *Genome Biol.* (2014) 15:550. doi: 10.1186/s13059-014-0550-8
18. Robinson MD, McCarthy DJ, Smyth GK. edgeR: a bioconductor package for differential expression analysis of digital gene expression data. *Bioinformatics.* (2010) 26:139–40. doi: 10.1093/bioinformatics/btp616
19. Bai Y, Li X, Chen Z, Li J, Tian H, Ma Y, et al. Interference with ACSL1 gene in bovine adipocytes: transcriptome profiling of mRNA and lncRNA related to unsaturated fatty acid synthesis. *Front Vet Sci.* (2021) 8:788316. doi: 10.3389/fvets.2021.788316
20. Park SJ, Beak SH, Jung DJS, Kim SY, Jeong IH, Piao MY, et al. Genetic, management, and nutritional factors affecting intramuscular fat deposition in beef cattle - a review. *Asian Australas J Anim Sci.* (2018) 31:1043–61. doi: 10.5713/ajas.18.0310
21. Luo M, Li T, Sang H. The role of hypoxia-inducible factor 1 $\alpha$  in hepatic lipid metabolism. *Mol Med.* (2023) 101:487–500. doi: 10.1007/s00109-023-02308-5
22. Liang C, Wang G, Raza SHA, Wang X, Li B, Zhang W, et al. FAM13A promotes proliferation of bovine preadipocytes by targeting hypoxia-inducible factor-1 signaling pathway. *Adipocytes.* (2021) 10:546–57. doi: 10.1080/21623945.2021.1986327
23. Wang Y, Nakajima T, Gonzalez FJ, Tanaka N. PPARs as metabolic regulators in the liver: lessons from liver-specific PPAR-null mice. *Int J Mol Sci.* (2020) 17:2061. doi: 10.3390/ijms21062061
24. Gregoire FM, Smas CM, Sul HS. Understanding adipocyte differentiation. *Physiol Rev.* (1998) 78:783–809. doi: 10.1152/physrev.1998.78.3.783
25. Prentice KJ, Saksi J, Hotamisligil GS. Adipokine FABP4 integrates energy stores and counterregulatory metabolic responses. *J Lipid Res.* (2019) 60:734–40. doi: 10.1194/jlr.S091793
26. Xiao C, Sun T, Yang Z, Zou L, Deng J, Yang X. Whole-transcriptome RNA sequencing reveals the global molecular responses and circRNA/lncRNA-miRNA-mRNA ceRNA regulatory network in chicken fat deposition. *Poult Sci.* (2022) 101:102121. doi: 10.1016/j.psj.2022.102121
27. Yousuf S, Li A, Feng H, Lui T, Huang W, Zhang X, et al. Genome-wide expression profiling and networking reveals an imperative role of IMF-associated novel CircRNAs as ceRNA in pigs. *Cells.* (2022) 11:2638. doi: 10.3390/cells11172638
28. Jiang Y, Liu J, Liu H, Zhang W, Li X, Liu L, et al. *mir-381-3p* inhibits intramuscular fat deposition through targeting *FABP3* by ceRNA regulatory network. *Biology.* (2022) 11:1497. doi: 10.3390/biology11101497
29. Tian X, Yan C, Liu M, Zhang Q, Liu D, Liu Y, et al. CREG1 heterozygous mice are susceptible to high fat diet-induced obesity and insulin resistance. *PLoS One.* (2017) 12:e0176873. doi: 10.1371/journal.pone.0176873

30. Zhang QY, Zhao LP, Tian XX, Yan CH, Li Y, Liu YX, et al. The novel intracellular protein CREG inhibits hepatic steatosis, obesity, and insulin resistance. *Hepatology*. (2017) 66:834–54. doi: 10.1002/hep.29257
31. Agnihotri G, Liu HW. Enoyl-CoA hydratase: reaction, mechanism, and inhibition. *Bioorg Med Chem*. (2003) 11:9–20. doi: 10.1016/S0968-0896(02)00333-4
32. Sharma NK, Chuang Key CC, Civelek M, Wabitsch M, Comeau ME, Langefeld CD, et al. Genetic regulation of Enoyl-CoA hydratase domain-containing 3 in adipose tissue determines insulin sensitivity in African Americans and Europeans. *Diabetes*. (2019) 68:1508–22. doi: 10.2337/db18-1229
33. Jones DE, Perez L, Ryan RO. 3-Methylglutaric acid in energy metabolism. *Clin Chim Acta*. (2020) 502:233–9. doi: 10.1016/j.cca.2019.11.006
34. Zheng ZM, Wang YY, Chen M, Yang HL, Lai ZZ, Li MQ, et al. FBXO17 inhibits the Wnt/ $\beta$ -catenin pathway and proliferation of Ishikawa cells. *Int J Med Sci*. (2022) 19:1430–41. doi: 10.7150/ijms.60335
35. Gao X, Wang Y, Zhao H, Wei F, Zhang X, Su Y, et al. Plasma miR-324-3p and miR-1285 as diagnostic and prognostic biomarkers for early stage lung squamous cell carcinoma. *Oncotarget*. (2016) 7:59664–75. doi: 10.18632/oncotarget.11198
36. Borrelli N, Denaro M, Ugolini C, Poma AM, Miccoli M, Vitti P, et al. MiRNA expression profiling of 'noninvasive follicular thyroid neoplasms with papillary-like nuclear features' compared with adenomas and infiltrative follicular variants of papillary thyroid carcinomas. *Mod Pathol*. (2017) 30:39–51. doi: 10.1038/modpathol.2016.157
37. An X, Li T, Chen N, Wang H, Su M, Shi H, et al. miR-1285-3p targets TPI1 to regulate the glycolysis metabolism signaling pathway of Tibetan sheep Sertoli cells. *PLoS One*. (2022) 17:e0270364. doi: 10.1371/journal.pone.0270364
38. Long JK, Dai W, Zheng YW, Zhao SP. miR-122 promotes hepatic lipogenesis via inhibiting the LKB1/AMPK pathway by targeting Sirt1 in non-alcoholic fatty liver disease. *Mol Med*. (2019) 25:26. doi: 10.1186/s10020-019-0085-2
39. Kang M, Liu X, Fu Y, Timothy Garvey W. Improved systemic metabolism and adipocyte biology in miR-150 knockout mice. *Metabolism*. (2018) 83:139–48. doi: 10.1016/j.metabol.2017.12.018
40. Ma X, Wei D, Cheng G, Li S, Wang L, Wang Y, et al. Bta-miR-130a/b regulates preadipocyte differentiation by targeting PPAR $\gamma$  and CYP2U1 in beef cattle. *Mol Cell Probes*. (2018) 42:10–7. doi: 10.1016/j.mcp.2018.10.002
41. Wang GL, Semenza GL. Purification and characterization of hypoxia-inducible factor 1. *J Biol Chem*. (1995) 270:1230–7. doi: 10.1074/jbc.270.3.1230
42. Jaakkola P, Mole DR, Tian YM, Wilson MI, Gielbert J, Gaskell SJ, et al. Targeting of HIF- $\alpha$  to the von Hippel-Lindau ubiquitylation complex by O<sub>2</sub>-regulated prolyl hydroxylation. *Science*. (2001) 292:468–72. doi: 10.1126/science.1059796
43. Yu F, White SB, Zhao Q, Lee FS. HIF-1 $\alpha$  binding to VHL is regulated by stimulus-sensitive proline hydroxylation. *Proc Natl Acad Sci U S A*. (2001) 98:9630–5. doi: 10.1073/pnas.181341498
44. Wang GL, Jiang BH, Rue EA, Semenza GL. Hypoxia-inducible factor 1 is a basic-helix-loop-helix-PAS heterodimer regulated by cellular O<sub>2</sub> tension. *Proc Natl Acad Sci U S A*. (1995) 92:5510–4. doi: 10.1073/pnas.92.12.5510
45. Gassmann M, Chilov D, Wenger RH. Induction and nuclear translocation of hypoxia-inducible factor-1 (HIF-1): heterodimerization with ARNT is not necessary for nuclear accumulation of HIF-1 $\alpha$ . *J Cell Sci*. (1999) 112:1203–12. doi: 10.1242/jcs.112.8.1203
46. Harris AL. Hypoxia — a key regulatory factor in tumour growth. *Nat Rev Cancer*. (2002) 2:38–47. doi: 10.1038/nrc704
47. Semenza GL. Targeting HIF-1 for cancer therapy. *Nat Rev Cancer*. (2003) 3:721–32. doi: 10.1038/nrc1187
48. Dengler VL, Galbraith M, Espinosa JM. Transcriptional regulation by hypoxia inducible factors. *Crit Rev Biochem Mol Biol*. (2014) 49:1–15. doi: 10.3109/10409238.2013.838205
49. Ge Q, Guo Y, Zheng W, Zhao S, Cai Y, Qi X. Molecular mechanisms detected in yak lung tissue via transcriptome-wide analysis provide insights into adaptation to high altitudes. *Sci Rep*. (2021) 11:7786. doi: 10.1038/s41598-021-87420-7
50. Ayalew W, Chu M, Liang C, Wu X, Yan P. Adaptation mechanisms of yak (*Bos grunniens*) to high-altitude environmental stress. *Animals*. (2021) 11:2344. doi: 10.3390/ani11082344
51. Liu Y, Ma Z, Zhao C, Wang Y, Wu G, Xiao J, et al. HIF-1 $\alpha$  and HIF-2 $\alpha$  are critically involved in hypoxia-induced lipid accumulation in hepatocytes through reducing PGC-1 $\alpha$ -mediated fatty acid  $\beta$ -oxidation. *Toxicol Lett*. (2014) 226:117–23. doi: 10.1016/j.toxlet.2014.01.033
52. Lee YS, Kim JW, Osborne O, Oh DY, Sasik R, Schenk S, et al. Increased adipocyte O<sub>2</sub> consumption triggers HIF-1 $\alpha$ , causing inflammation and insulin resistance in obesity. *Cells*. (2014) 157:1339–52. doi: 10.1016/j.cell.2014.05.012
53. Xiong X, Fu M, Lan D, Li J, Zi X, Zhong J. Yak response to high-altitude hypoxic stress by altering mRNA expression and DNA methylation of hypoxia-inducible factors. *Anim Biotechnol*. (2015) 26:222–9. doi: 10.1080/10495398.2014.1002563
54. Muñoz-Sánchez J, Cháñez-Cárdenas ME. The use of cobalt chloride as a chemical hypoxia model. *J Appl Toxicol*. (2019) 39:556–70. doi: 10.1002/jat.3749
55. Kakudo N, Morimoto N, Ogawa T, Taketani S, Kusumoto K. Hypoxia enhances proliferation of human adipose-derived stem cells via HIF-1 $\alpha$  activation. *PLoS One*. (2015) 10:e0139890. doi: 10.1371/journal.pone.0139890
56. Yamamoto Y, Fujita M, Tanaka Y, Kojima I, Kanatani Y, Ishihara M, et al. Low oxygen tension enhances proliferation and maintains stemness of adipose tissue-derived stromal cells. *Biores Open Access*. (2013) 2:199–205. doi: 10.1089/biores.2013.0004
57. Du W, Zhang L, Brett-Morris A, Aguila B, Kerner J, Hoppel CL, et al. HIF drives lipid deposition and cancer in ccRCC via repression of fatty acid metabolism. *Nat Commun*. (2017) 8:1769. doi: 10.1038/s41467-017-01965-8
58. Peng C, Peil H, Wei F, Tian X, Deng J, Yan C, et al. Cellular repressor of E1A-stimulated gene overexpression in bone mesenchymal stem cells protects against rat myocardial infarction. *Int J Cardiol*. (2015) 183:232–41. doi: 10.1016/j.ijcard.2015.01.059